REPORT DOCUMENTATION PAGE

Form Approved
OMB No. 0704-0188

PLEASE DO NOT RETURN YOUR FORM TO THE ABOVE ORGANIZATION.

1. REPORT DATE *(DD-MM-YYYY)*	2. REPORT TYPE	3. DATES COVERED *(From - To)*
11-03-2011	Final Technical	01-01-2008 -- 12-31-2010

4. TITLE AND SUBTITLE

Advanced CFD Methods for Hypervelocity Wind Tunnels

5a. CONTRACT NUMBER

5b. GRANT NUMBER

FA9550-08-1-0397

5c. PROGRAM ELEMENT NUMBER

6. AUTHOR(S)

Graham V. Candler

5d. PROJECT NUMBER

5e. TASK NUMBER

5f. WORK UNIT NUMBER

7. PERFORMING ORGANIZATION NAME(S) AND ADDRESS(ES)

University of Minnesota
110 Union Street SE
Minneapolis, MN 55455

8. PERFORMING ORGANIZATION REPORT NUMBER

9. SPONSORING/MONITORING AGENCY NAME(S) AND ADDRESS(ES)

AFOSR
875 North Randolph Street
Suite 325, Rm 3112
Arlington, VA 22203

10. SPONSOR/MONITOR'S ACRONYM(S)

11. SPONSOR/MONITOR'S REPORT NUMBER(S)

AFRL-OSR-VA-TR-2012-0875

12. DISTRIBUTION/AVAILABILITY STATEMENT

Distribution A

13. SUPPLEMENTARY NOTES

14. ABSTRACT

There are two main components of the work performed during this project. First, a finite-rate vibrational energy relaxation model was developed to study how the possible presence of water vapor in the Tunnel 9 facility could affect the flow properties. We find that water vapor levels at about 500 parts per million (ppm) could cause appreciable relaxation of the nitrogen test gas, however, even at these large levels, the effect on the flow quality is minimal. Secondly, a novel grid generation scheme for hypersonic nozzle flows is presented. The grid is based on the characteristic lines of the supersonic regions of the flow. This allows for grid alignment and clustering along shock waves present in the flow. Results from simulations run on the AEDC Hypervelocity Tunnel 9 Mach 14 nozzle give good agreement with simulations performed using a conventional grid. Some results from an investigation into the effect of wall contour discontinuities present in the Mach 14 Nozzle are presented. Avenues for future research into flow irregularities in the Mach 14 nozzle are outlined.

15. SUBJECT TERMS

Hypersonic flow, hypervelocity, wind tunnel operation

16. SECURITY CLASSIFICATION OF:			17. LIMITATION OF ABSTRACT	18. NUMBER OF PAGES	19a. NAME OF RESPONSIBLE PERSON
a. REPORT	b. ABSTRACT	c. THIS PAGE			Graham V. Candler
U	U	U	UU	23	19b. TELEPHONE NUMBER *(Include area code)* 612-625-2364

Final Report for AFOSR Grant FA9550-08-1-0397

Advanced CFD Methods for Hypervelocity Wind Tunnel Nozzles

Graham V. Candler

110 Union Street SE
Department of Aerospace Engineering & Mechanics
University of Minnesota
Minneapolis, MN, 55455

March 10, 2011

Contents

1 Abstract

There are two main components of the work performed during this project. First, a finite-rate vibrational energy relaxation model was developed to study how the possible presence of water vapor in the Tunnel 9 facility could affect the flow properties. We find that water vapor levels at about 500 parts per million (ppm) could cause appreciable relaxation of the nitrogen test gas, however, even at these large levels, the effect on the flow quality is minimal. Secondly, a novel grid generation scheme for hypersonic nozzle flows is presented. The grid is based on the characteristic lines of the supersonic regions of the flow. This allows for grid alignment and clustering along shock waves present in the flow. Results from simulations run on the AEDC Hypervelocity Tunnel 9 Mach 14 nozzle give good agreement with simulations performed using a conventional grid. Some results from an investigation into the effect of wall contour discontinuities present in the Mach 14 Nozzle are presented. Avenues for future research into flow irregularities in the Mach 14 nozzle are outlined.

2 Introduction

Accurate predictions from computational fluid dynamics (CFD) simulations are essential to the design of hypersonic vehicles. In order to have confidence in the accuracy of CFD simulations, it is necessary to have experimental data to validate the CFD results, for example measurements from a wind tunnel. Thus, it is critical to ensure that the wind tunnel design is of the highest quality, and any non-uniformities in the nozzle flow are minimized. It is technically challenging to design a wind tunnel that can produce the hypervelocity flows that are required for these purposes.

The Arnold Engineering Development Center (AEDC) Hypervelocity Tunnel 9 is one of the nation's premiere hypersonic test facilities. The tunnel is large, has run times on the order of several seconds, and can be run from Mach 8 to Mach 14 across a wide range of unit Reynolds numbers. These factors make Tunnel 9 unique and useful for obtaining force and moment test data of hypersonic vehicle designs. However, the Mach 14 nozzle produces non-uniformities in the test section flow that are not desirable [1,2]. Calibration runs with Pitot pressure rakes suggest that a series of weak shock waves cross the test section, which appear as variations in the core flow Pitot profile.

A potential source of the non-ideal flow could be the presence of vibrational nonequilibrium in the flow of nitrogen in the AEDC Tunnel 9 nozzle. Standard vibrational relaxation models predict that the nitrogen test gas vibrational modes freeze close to the throat. However careful CARS (coherent anti-Raman scattering) measurements at the higher operating pressures show that there is no detectable vibrational excitation at Mach 10 and 14 [3,4]. The first part of the research project studied the effect of water vapor on the vibrational relaxation of the test gas in an attempt to understand this discrepancy between simulations and experiment.

Previous numerical studies of ideal smooth-surface flow in the Mach 14 nozzle do not show the presence of weak shock waves [1]. However, it is known that the nozzle as-built contour is not ideal, and in fact there are imperfect joints in the nozzle that cause small discontinuities in the wall contour. Studies that have included a representative model for similar joint imperfections in the Mach 8 nozzle indicate that the flow develops with weak shock waves passing through the test section [2]. Accurate numerical simulations that capture the effects of these geometric imperfections are challenging, as the waves are weak as compared to the expansion of the mean flow. Additionally, the waves are oblique to a conventional grid, and thus cross the grid cells in a way that is very numerically dissipative. In order to understand the influence of the weak shock waves, the grid must be extremely fine. Due to the large range of length scales present in the problem, even an axisymmetric simulation using a sufficiently fine grid of the Mach 14 nozzle would be beyond current computational capability.

This grant helped develop a novel grid generation approach to overcome the shortcomings of conventional CFD grids with respect to this problem, namely that conventional grids cannot predict the Pitot pressure distribution in the test section of the Mach 14 nozzle. Because the waves generated by the joint imperfections propagate along the characteristic lines of the flow, a grid in which the cells are aligned with the characteristics offers advantages over a conventional grid. With this grid, the weak shock waves do not cross the grid cells in an oblique manner, reducing numerical dissipation as compared to a conventional grid. Additionally, the grid cells can be clustered in the region of the shock waves, which greatly reduces the number of elements required in the simulation, while maintaining the necessary accuracy to capture the effect of the waves. This allows the simulations to be done at a reasonable computational cost.

This final report summarizes progress toward understanding the irregularities in the Mach 14 nozzle. Results of simulations aimed at capturing the effect of known joint imperfections on the nozzle flow will be shown, and avenues for future possible research are presented.

3 Statement of Objectives

1. Study the effect of water vapor on the vibrational energy relaxation of the test gas.

2. Development of grid generation code which aligns grid elements with characteristic lines in the flow of the Mach 14 nozzle
   a) Create lattice of grid points from intersection of characteristic lines of ideal geometry flow
   b) Create axisymmetric finite volume mesh from these grid points
   c) Add representative models for nozzle joint imperfections in the finite volume mesh; refine where necessary to capture effect of joints on flow physics

3. Simulate flow in Mach 14 nozzle with imperfect geometry at Re = 0.5M/ft using US3D
   a) Capture individual effects of both the step joint and the V-notch
   b) Investigate the interaction and combined effect of both joints

4. Analyze the data from the simulations
   a) Compare pitot pressure measurements to simulation results at various locations in the test cell

4 Research Effort

4.1 Introduction

The AEDC Hypervelocity Wind Tunnel Number 9 is located at the White Oak, Maryland test facility. It is a blowdown tunnel which uses nitrogen as the working fluid. Tunnel 9 is capable of being run with nozzles that can generate Mach 7, 8, 10, and 14 flows over a wide range of unit Reynolds numbers. The Mach 14 nozzle has been the nozzle of interest for this research due to the non-uniformity present in the test cell flow. The Mach 14 nozzle is 40 feet long with a 60-in. diameter exit, feeding into a test section that is over 12 feet long. The high Mach and Reynolds numbers capable in the Mach 14 nozzle, combined with its large size and long run times, make it possible to collect force and moment data over a wide range of angles during a single run. Thus, making progress toward understanding the non-uniformities present in the flow has been of utmost importance for this research.

Research was completed in simulating the Mach 14 nozzle with the known joint imperfections using the characteristics-based grid, in an attempt to resolve the weak shock waves present in the flow and determine quantitatively their effect on the test section. The simulations were axisymmetric and performed using the University of Minnesota's US3D code [5-7], a finite-volume Navier-Stokes solver. As the grid generation method is the novel aspect of this research, the specifics of the development of US3D are not presented here.

4.2 Effect of Water Vapor on Vibrational Relaxation

Meador, Townsend, and Miner [8] developed a model for the de-excitation of nitrogen in the presence of water vapor. They point out that water molecules have a special property that makes them very efficient quenchers of vibrational excitation. This is because of the geometry of the water molecule: two light hydrogen atoms bonded to a massive oxygen atom at nearly right angles. This makes the molecule’s moment of inertia small, with many closely spaced rotational levels. Thus, there are many near resonant energy matches between the vibrational levels of most molecules and the vibrational-rotational levels of water. In a hypersonic flow of nitrogen with a trace level of water vapor, the vibrationally excited nitrogen transfers its vibrational energy to the vibrational-rotational energy of water vapor through a very rapid process (a V-VR transition). Then the excited water vapor de-excites through vibrational-translational (V-T) transitions due to collisions with N_2. The two critical reactions are:

$$N_2^* + H_2O \rightarrow N_2 + H_2O^*$$
$$H_2O^* + N_2 \rightarrow H_2O + N_2$$

Here, the * superscript indicates a molecule that is excited to the first vibrational state above the ground state; the species without an asterisk are ground state molecules. Conventional CFD models of vibrational relaxation usually only include vibrational-translational (V-T) energy transitions. They typically do not include the very important V-VR process shown above, and as a result, under-predict the importance of water vapor on vibrational quenching.

We use an existing computational fluid dynamics code to study the effects of water vapor on the Tunnel 9 Mach 14 flow [9]. This code was designed for the analysis of hypersonic converging-diverging nozzles, and uses an excluded volume equation of state to model high-pressure non-ideal gas effects, along with a finite-rate thermo-chemical model for high-temperature reacting flows. As discussed above, the concentration of water vapor is known to strongly influence the vibrational relaxation of molecules, including that of nitrogen, which is used as a test gas in the facility. Therefore, the nozzle simulation code was modified to incorporate the presence of water and its interaction with the nitrogen test gas. We use the model due to Meador et al[8] with four chemical species (N_2, H_2O, N_2^*, and H_2O^*) and the following five reactions:

$$N_2^* + N_2 \leftrightarrow N_2 + N_2 \quad \text{(R1)}$$

$$N_2^* + H_2O \leftrightarrow N_2 + H_2O \quad \text{(R2)}$$

$$N_2^* + H_2O \leftrightarrow N_2 + H_2O^* \quad \text{(R3)}$$

$$H_2O^* + H_2O \leftrightarrow H_2O + H_2O \quad \text{(R4)}$$

$$H_2O^* + N_2 \leftrightarrow H_2O + N_2 \quad \text{(R5)}$$

The rates of these reactions were obtained from three separate sources. The rate constant for the first reaction (R1) originates from Vincenti and Kruger [10], and it can be derived from the relationship between the relaxation time and the rate constant for V-T transitions. The relaxation time, τ, is the time required for the difference in the total vibration energy to the equilibrium energy to reach $1/e$ of its initial value. For a simple harmonic oscillator, we have the following relationship between the relaxation time and the rate of V-T transitions from the $v = 1$ state to the $v = 0$ state, $k_{1,0}$:

$$\tau = \left[k_{1,0}\left(1 - e^{-\theta_v / T}\right)\right]^{-1} \quad (1)$$

Here θ_v is the characteristic temperature of vibration for the employed species. The data for nitrogen and water are known, and are given as: θ_v = 3395 K for N_2 and θ_v = 2295 K for H_2O.

The theoretical relaxation time as a function of temperature and pressure was first derived by Landau and Teller, which at sufficiently low temperatures can be represented to good approximation by:

$$p\tau = C \exp\left((K_2 / T)^{1/3}\right) \tag{2}$$

where C and K_2 are constants, the latter of which depends on the physical properties of the molecule in question. Constants for various species and heat-bath molecules are known, and for N_2 they are: $C = 7.12\text{x}10^{-3}$ atm-μsec and $K_2 = 1.91\text{x}10^6$ K.

Introducing the ideal gas law into Eqs. (1) and (2) gives the rate for the first reaction in the form usually used to quantify the rate of vibrational excitation or de-excitation. This expression has units of inverse seconds per atmosphere of pressure of the relevant species. As we will see, we must convert these units to those required for the chemical kinetics model. This reaction rate is (in s^{-1} atm^{-1}):

$$\tilde{k}_{R1} = \frac{\exp\left(-(K_2 / T)^{1/3}\right)}{C\left(1 - e^{-\theta_{vN_2} / T}\right)} \tag{3}$$

Bass [11] gives the rate constants for the three reactions R2, R4, and R5 as:

$$\tilde{k}_{R2} = 9.0 \times 10^6 \; e^{-28.4/T^{1/3}} \tag{4}$$

$$\tilde{k}_{R4} = 38.5 \; e^{113.5/T^{1/3}} \text{ for } T < 410 \text{ K} \tag{5}$$

$$\tilde{k}_{R4} = 1.4 \times 10^8 \text{ for } T > 410 \text{ K} \tag{6}$$

$$\tilde{k}_{R5} = 2.8 \times 10^9 \; e^{-51.3/T^{1/3}} \tag{7}$$

Finally, Nagel and Rogovin [12] give the rate constant for the remaining reaction in the model (R3):

$$\tilde{k}_{R3} = 2.557 \times 10^7 \; e^{-27/T^{1/3}} \text{ for } T < 750 \text{ K} \tag{8}$$

$$\tilde{k}_{R3} = 2.878 \times 10^9 \; e^{-69.9/T^{1/3}} \text{ for T} > 750 \text{ K} \tag{9}$$

Now we must convert these rates to the conventional form used for chemical kinetics. To do so, consider a reaction of the form:

$$N_2^* + S \rightarrow N_2 + S \tag{10}$$

where S is a collision partner. In the forward direction the rate of formation of species N_2 is conventionally written in the form (with the reaction rate in units of m^3 / kmole sec).

$$\frac{d\rho_{N_2}}{dt} = M_{N_2} \frac{\rho_{N_2^*}}{M_{N_2^*}} \frac{\rho_S}{M_S} k_f \tag{11}$$

However, the reaction rates given above assume a form of the reaction given by:

$$\frac{dN_{N_2}}{dt} = N_S \, \tilde{k} \tag{12}$$

Where for this reaction, we have:

$$\tilde{k} = p_{N_2^*} A \exp(B / T^{1/3}) = \rho_{N_2^*} \frac{\hat{R}}{M_{N_2^*}} T \, A \exp(B / T^{1/3}) \tag{13}$$

Comparing these expressions shows that the kinetic rate constant is given by:

$$k_f = \hat{R} T \, \tilde{k} \tag{14}$$

Where the universal gas constant has the appropriate units ($\hat{R} = 0.082056$ m^3 atm / kmole K).

Now we must determine the backward reaction rates for each of the reactions given above. We can use the equilibrium constant, which is given as:

$$K_{eq} = \frac{k_f}{k_b} \tag{15}$$

where k_b is the backward reaction rate. The equilibrium constant can be evaluated through the ratio of molecules that occupy some energy state of vibration, denoted by i, to the total number of molecules present:

$$\frac{N_i}{N} = e^{-\varepsilon_i / kT} / \sum_i e^{-\varepsilon_i / kT} \tag{16}$$

where N_i is the total population of energy state i, N is the total number of molecules, ε_i is the

vibrational energy of state i, and k is the Boltzmann constant. It can be shown that the equilibrium constant for each reaction is written as follows:

$$(K_{eq})_{R1} = (K_{eq})_{R2} = e^{\theta_{vN_2}/T} \tag{17}$$

$$(K_{eq})_{R3} = e^{(\theta_{vN_2} - \theta_{vH_2O})/T} \tag{18}$$

$$(K_{eq})_{R4} = (K_{eq})_{R5} = e^{\theta_{vH_2O}/T} \tag{19}$$

With these expressions, we can develop the complete set of forward and backward reaction rates for each reaction. These have been implemented in the nozzle code, [9] and verified by comparison to zero-dimensional relaxation results using the same kinetics model.

With this thermo-chemical model it is necessary to compute the mass fraction of the gas in its initial state in the reservoir of the tunnel. Using the expressions for the equilibrium constant leads to relationships between the mass fractions of the ground state and excited molecules for each species:

$$\frac{c_{N_2^*}}{c_{N_2}} = e^{-\theta_{vN_2}/T}, \quad \frac{c_{H_2O^*}}{c_{H_2O}} = e^{-\theta_{vH_2O}/T} \tag{20}$$

where c_s is the mass fraction of species s. Therefore, given an assumed mass fraction of water in the Tunnel 9 test gas we have the means with which to determine the remaining initial constituents in the gas. From this point the relevant analysis has been completed to allow full implementation of the chemistry model in the nozzle simulation code.

The Mach 14 Tunnel 9 nozzle geometry was represented with a 300 by 120 computational grid, including the portion of the nozzle upstream of the throat. The baseline conditions considered represent the low Reynolds number Tunnel 9 operating conditions of 2025 psi (14.0 MPa) and 2777 R (1543 K). Cases with pure N_2 and increasing levels of H_2O were run to assess the effects of water vapor on the relaxation of the gas at these conditions.

Figure 1 (upper) plots the nozzle centerline translational-rotational and N_2 and H_2O vibrational temperatures for the baseline conditions; the simulations were run with varying levels of water vapor from pure N_2 to a mole fraction of 0.005 (0.5%). Here the vibrational temperatures are computed using the ratio of the excited to ground state mass fractions, as given in Eq. (20). Note that increasing levels of water vapor do indeed relax the vibrational modes of the gas. Also, because of the rapid expansion, the relaxation process occurs in the throat region, and the relaxation process is frozen for almost the entire length of the nozzle. Table 1 presents the centerline nozzle exit plane conditions for this case. These results show that increasing levels of

relaxation increase the translation-rotational temperature, as expected. There is little effect on the resulting centerline Mach number.

It should be noted that the use of temperature (rather than energy) to quantify the vibrational nonequilibrium is somewhat misleading. The vibrational energy is non-linear in vibrational temperature, as shown in Fig. 2. Thus, an apparent strong level of vibrational nonequilibrium based on T, only translates to a small level of energy storage in the vibrational energy modes. Once T_{vN2} is below about 600 K, there is virtually no energy stored in the vibrational energy modes. Furthermore, it is difficult, if not impossible, to use CARS to detect vibrational energy at low levels of vibrational energy. The approach used by Smith cannot detect vibrational excitation below about 700 K [3,4]. Thus, even quite small levels of water vapor (0.05% mole fraction or 500 ppm) could be responsible for the apparent lack of vibrational nonequilibrium in the measurements of Smith.

Figure 1 (lower) plots the same results for a higher stagnation pressure condition of 8750 psi (60.3 MPa) and 2960 R (1644 K). At this higher pressure condition, the pure nitrogen gas relaxes more quickly and lower levels of water are required to drive the N_2 vibrational energy close to equilibrium. Again, small levels of water vapor could cause vibrational relaxation of the N_2 gas.

Figure 3 plots the computed exit-plane Pitot pressure non-dimensionalized by the reservoir pressure for the two cases. Note that the enhanced vibrational relaxation caused by the presence of water vapor does not affect the Pitot pressure to any appreciable degree. Thus, if there is water vapor present in the supply gas, it does not affect the operation of the facility. This can be further confirmed by considering how the exit-plane Mach number an velocity vary, as given in Tables 1 and 2. Therefore, this analysis shows that the issues with flow uniformity are unlikely to be caused by vibrational relaxation effects.

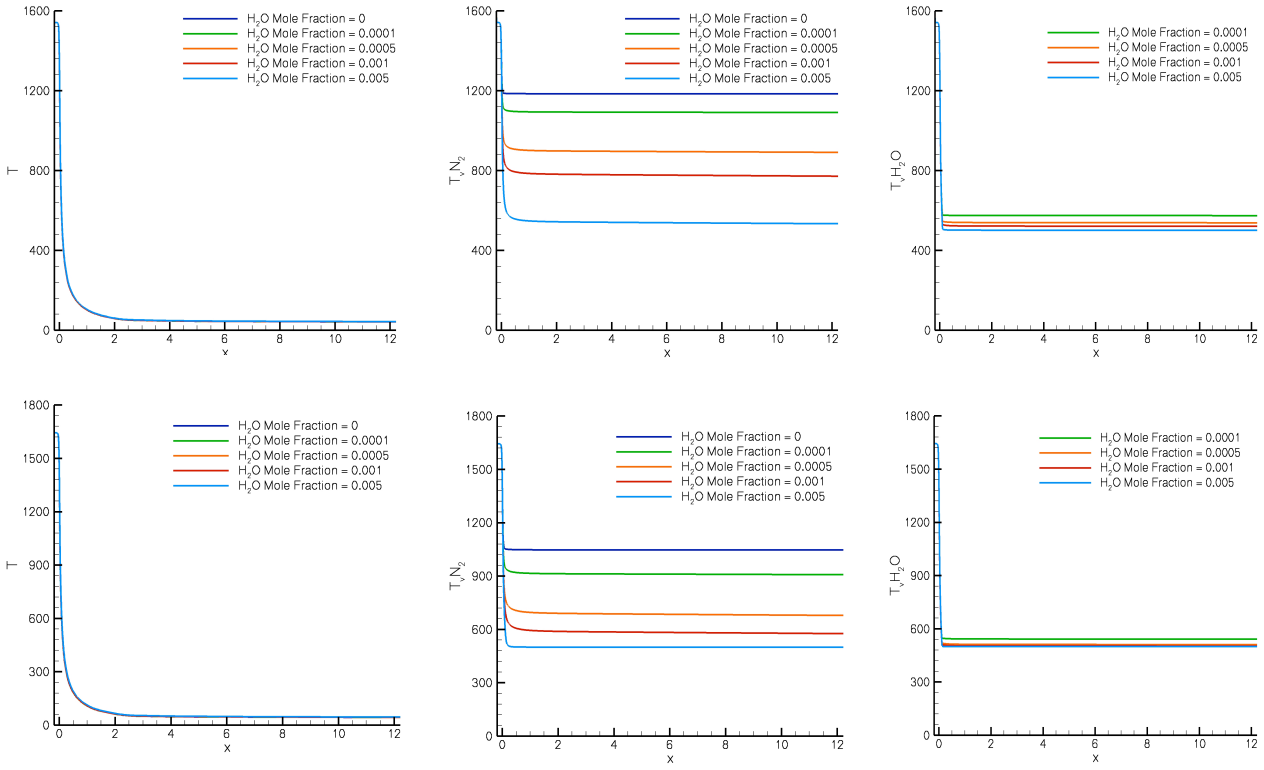

Figure 1: Centerline translational-rotational temperature (left), N_2 vibrational temperature (center) and H_2O vibrational temperature (right). Upper: Case 1 conditions (2025 psi and 2777 R); Lower: Case 2 conditions (8750 psi and 2960 R).

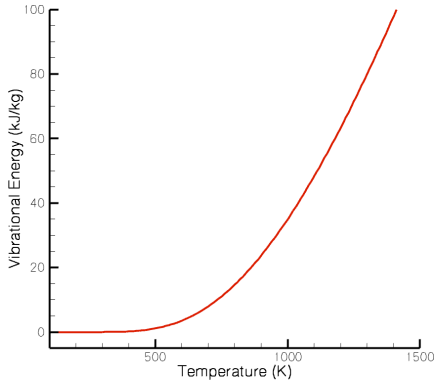

Figure 2: N_2 vibrational energy as a function of temperature.

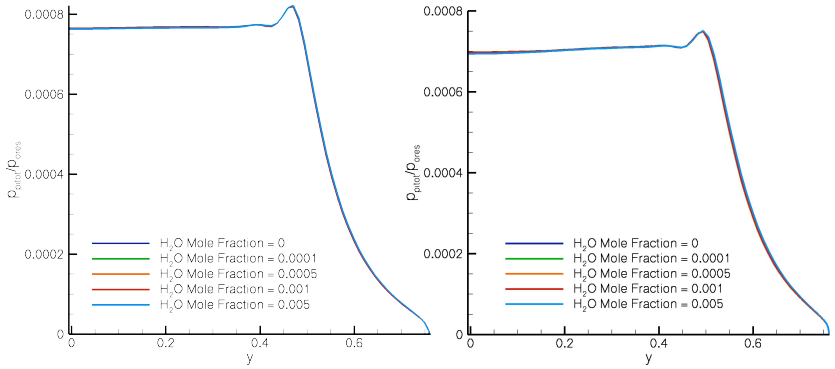

Figure 3. Non-dimensionalized Pitot pressure at the nozzle exit plane for the two cases computed; Case 1 (left), Case 2 (right).

Table 1. Exit-plane conditions for Case 1.

H_2O Mole Fraction	T (K)	T_{vN2} (K)	T_{vH2O} (K)	u (m/s)	M
0	**41.9**	**1542**	**--**	**1784**	**13.52**
0.0001	**41.1**	**1213**	**598**	**1785**	**13.52**
0.0005	**42.1**	**917**	**542**	**1787**	**13.51**
0.001	**42.3**	**782**	**522**	**1790**	**13.50**
0.005	**43.3**	**534**	**501**	**1804**	**13.43**

Table 2. Exit-plane conditions for Case 2.

H_2O Mole Fraction	T (K)	T_{vN2} (K)	T_{vH2O} (K)	u (m/s)	M
0	**43.3**	**1047**	**--**	**1884**	**14.04**
0.0001	**43.4**	**908**	**542**	**1885**	**14.03**
0.0005	**43.7**	**679**	**511**	**1889**	**14.01**
0.001	**44.0**	**577**	**503**	**1893**	**13.99**
0.005	**45.5**	**500**	**500**	**1911**	**13.88**

4.3 Generation of the characteristics-based grid

The generation of a grid aligned with the characteristics of the flow is extremely important. The unique aspects of this grid allow the shocks to be resolved by the flow solver in a manageable computation time. In order to create the grid, knowledge of certain flow field variables is necessary. To obtain these variables, the solver is first run on an ideal nozzle geometry. This provides distributions of Mach number and flow angle over physical space, from which the characteristics of the flow can be obtained. Note that by adding contour discontinuities to the nozzle wall, the characteristics are not appreciably affected. The effect of the shock waves generated at the joints is much weaker than the expansion of the mean flow, and thus the characteristics are dominated by the nominal nozzle geometry.

Once a solution for the ideal flow has been obtained, the characteristic grid can be generated. To begin with, an initial line of grid points perpendicular to the nozzle axis is created at a location downstream of the nozzle throat. This is necessary because the characteristics are only real for regions where the flow is locally supersonic. Upstream of this point, a body-fitted Cartesian grid is used. Characteristic lines from each of these initial grid points can be created as rays originating from the point. Each point has a left and right-leaning characteristic line. The angle of the characteristics are calculated as follows:

$$\alpha = \theta \pm \mu \tag{21}$$

where α is the characteristic angle, θ is the flow angle, and μ is the Mach angle. The positive sign

corresponds to the right leaning characteristic while the negative corresponds to the left leaning characteristic. The flow angle is determined by the ratio of the local x and y components of fluid velocity, while the Mach angle is determined by the local Mach number:

$$\theta = \arctan\left(\frac{v}{u}\right) \tag{22}$$

$$\mu = \arcsin\left(\frac{1}{M}\right) \tag{23}$$

The slope of the lines emanating from a grid point are found by taking the inverse tangent of the characteristic angle. The right leaning line has a positive slope and the left leaning line a negative slope. Thus, from the initial distribution of grid points a new set of grid points further downstream is found by finding the intersection of the calculated characteristic lines. This process is repeated marching downstream along the nozzle axis and through the test section. The resulting set of grid points can then be used to create an unstructured grid of almost exclusively hexahedral elements, the exception being elements located on the centerline which are necessarily prismatic.

Near the wall, as the Mach number decreases, the characteristic lines curve toward the wall and eventually intersect the wall at an angle normal to the local contour. To model this behavior, the characteristic lines of the grid do not reflect off of the physical wall, but rather somewhere located in the Mach number boundary layer. Between this reflection line and the wall, a layer of structured hexahedral elements is used with clustering at the surface. Because it is not possible to know exactly where the reflection line should be set ahead of time, the simulation may have to be run several times in order to ensure that the characteristic grid elements are aligned with the waves present in the flow for the entire length of the nozzle.

Note that when selecting the initial distribution of grid points, regular spacing is not necessary. Clustering of these initial points results in grid cell clustering, and this can be done in such a way as to refine the characteristic grid at the location of the weak shock waves. As the characteristic lines do not dissipate, this method allows for grid refinement near the waves for the entire length of the nozzle without requiring an inordinate number of grid elements. Figures 4-6 show several images of the characteristics-based grid.

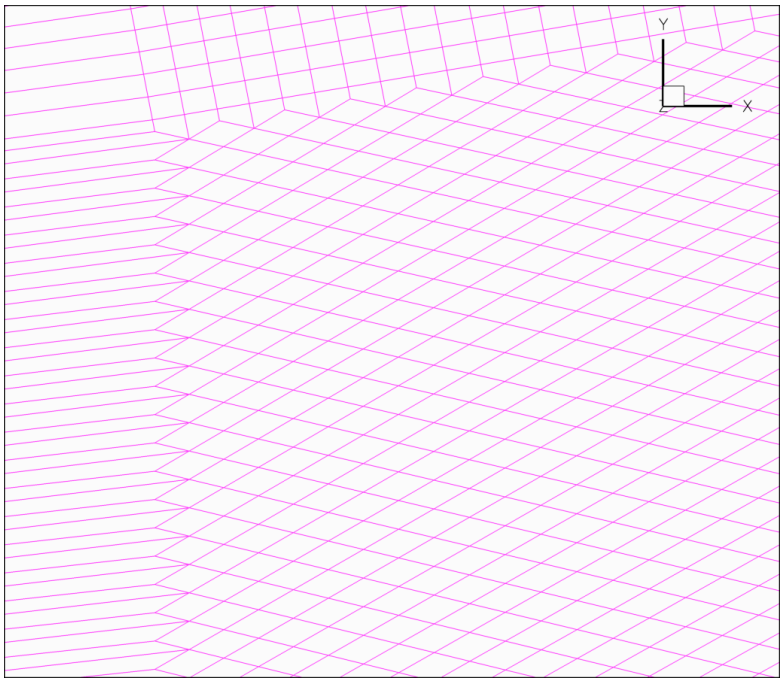

Figure 4. Characteristic lines are traced out once the flow becomes supersonic.

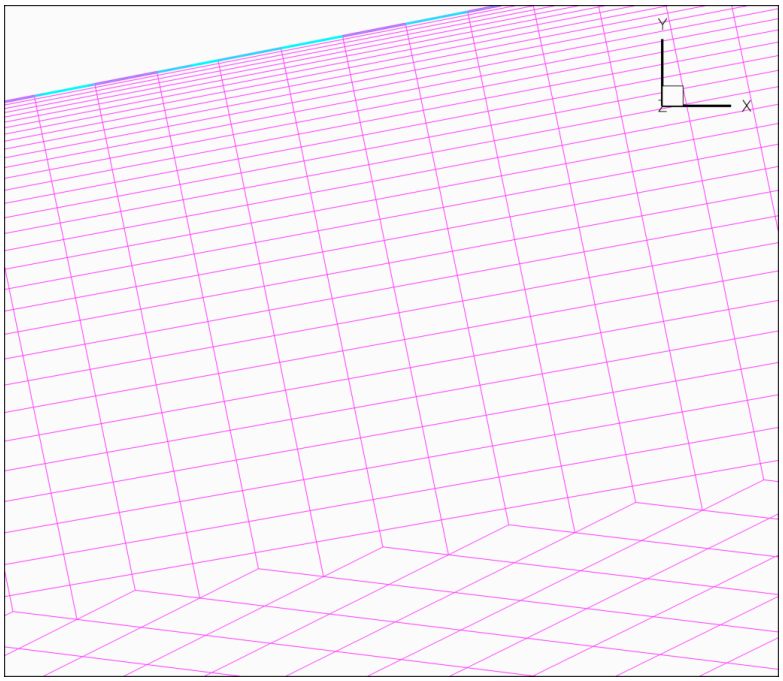

Figure 5. Reflection of characteristic lines at the nozzle wall.

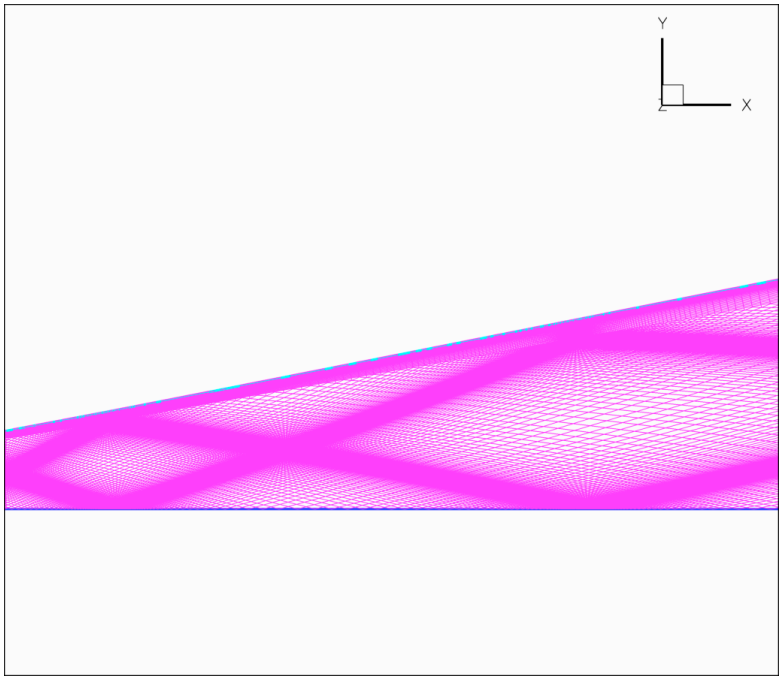

Figure 6. Clustering of grid elements along characteristic lines.

Simulations have been conducted to compare the performance of the characteristics based grid with a conventional grid. The boundary conditions used are the same for all simulations. At the inlet, a subsonic boundary condition based on a total enthalpy calculation is applied, and a supersonic boundary condition is applied at the outflow. The no-slip condition is applied at the wall for flow velocity, and wall temperature is read in from a file and interpolated along the nozzle axial direction. All simulations are axisymmetric.

The gas used in all simulations is nitrogen. The nozzle reservoir parameters are: pressure of 14.7 MPa, temperature of 16.39 K and density of 29.23 kg/m^3. These reservoir parameters correspond to a unit Reynolds number of approximately 0.5 x 10^6 per foot in the test cell as measured experimentally.

Figure 7 compares the simulation results for ideal flow using a conventional body-fitted structured grid and the characteristics grid. The agreement between the two grids for this case is excellent, lending confidence to the decision to use the characteristics grid to simulate the effects of the nozzle joint.

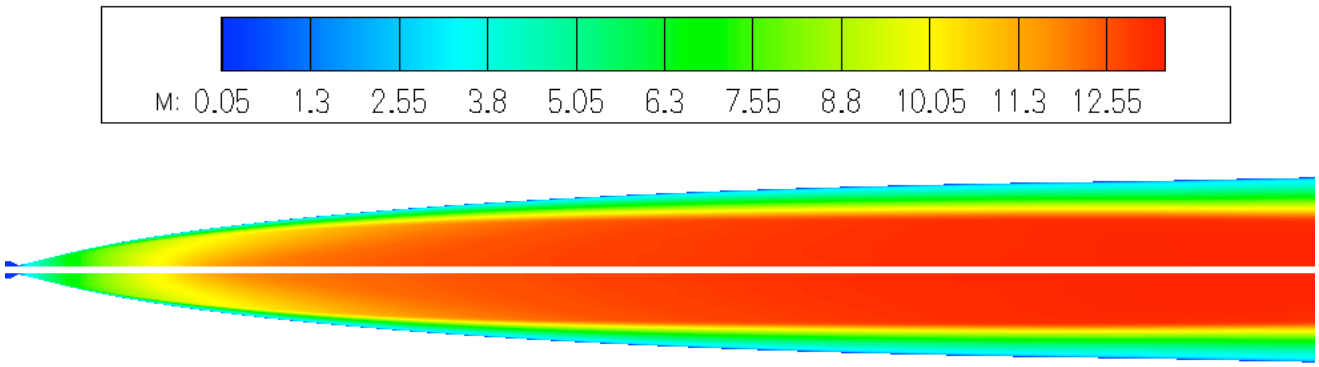

Figure 7. Top: Mach number contours using a conventional grid. Bottom: Characteristic grid.

4.4 Results

Simulations have been performed in an attempt to analyze the effect of the nozzle joint imperfections. Due to high wall temperatures in the region of the throat, the nozzle throat piece shrinks inward due to thermal expansion. The stresses associated with this expansion can cause a discontinuity that manifests itself as a rearwards-facing step that can grow in height to the order of 1mm, located 71.6 mm downstream of the nozzle throat. Simulations were performed using a somewhat typical step height of 0.5 mm. Additionally, there is a .010" wide V-notch located 234 mm downstream of the throat. Figures 8 and 9 demonstrate how refining the characteristics based grid is done to resolve the flow at the locations of the joint imperfections.

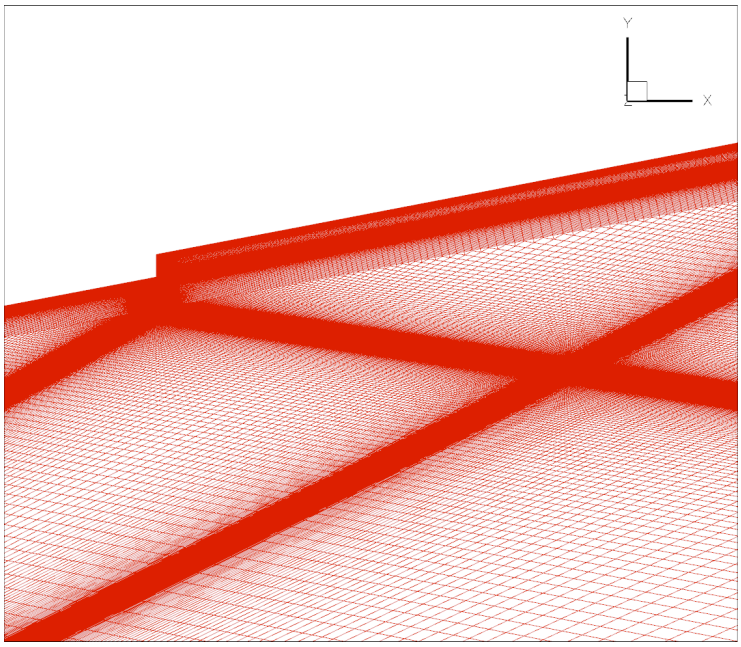

Figure 8. Grid refinement near the backward facing step and along the wave generated by the step.

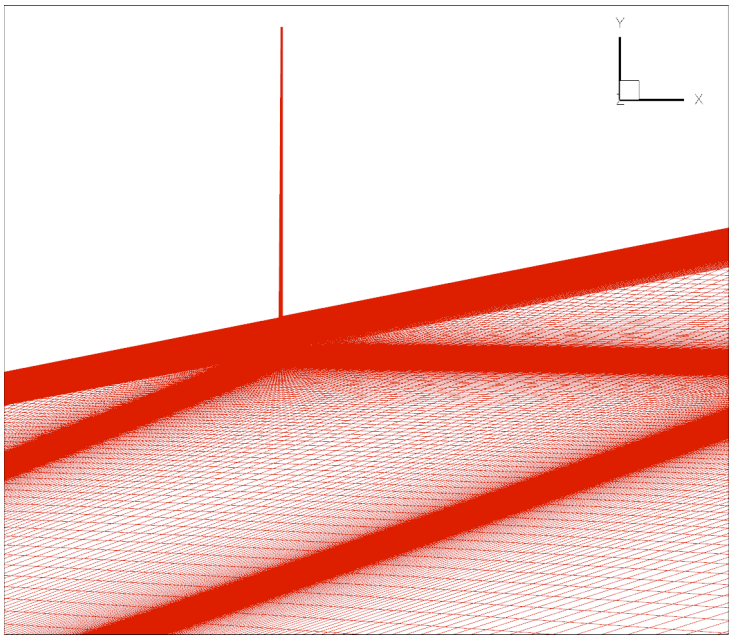

Figure 9. Grid refinement near the v-notch and along the wave generated by the notch.

4.4.1 Presence of Waves Generated by Joint Imperfections

Figure 10 shows the steady state Mach number distribution for a simulation run with the 0.5 mm step. As predicted, the presence of the step generates weak shock waves that travel down the length of the nozzle. It has been suspected that these waves are responsible for losses and non-uniformities of Pitot pressure in the test cell. Figure 11 shows how the centerline Mach number varies with axial position for cases run with the two joint imperfections individually.

It is clear that the waves generated by the imperfect nozzle geometry cause significant deviations from the nominal flow. Figure 12 shows centerline Mach and Pitot pressure data for a simulation in which both joints were modeled together. This figure demonstrates that the effect of both joints can be captured simultaneously, and there appears to be some interaction effect between the waves, as the Mach number does not behave the same as in the isolated cases.

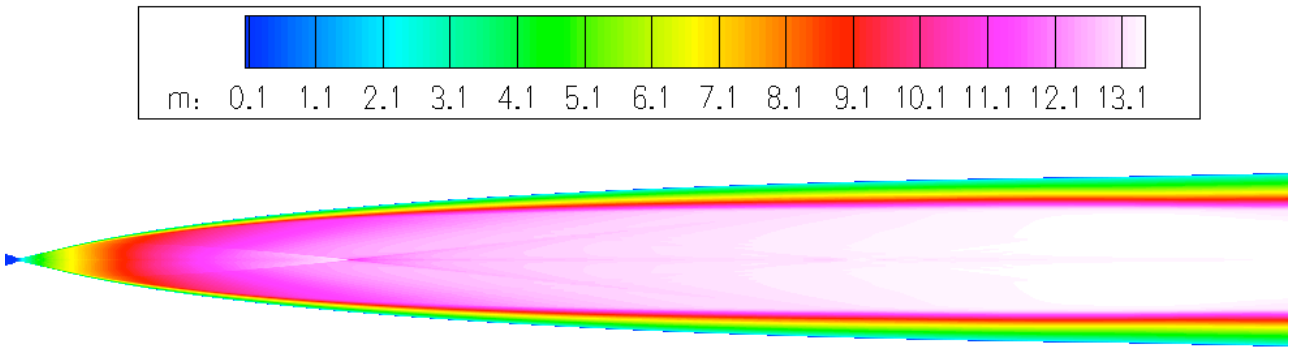

Figure 10. Mach number contours showing the presence of weak shock waves generated by the step.

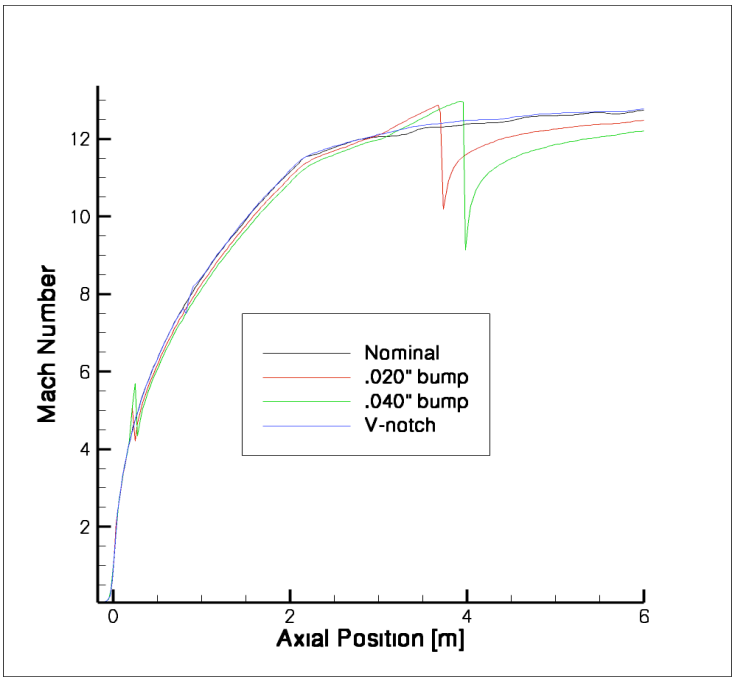

Figure 11. Centerline Mach number for simulations with non-ideal geometries.

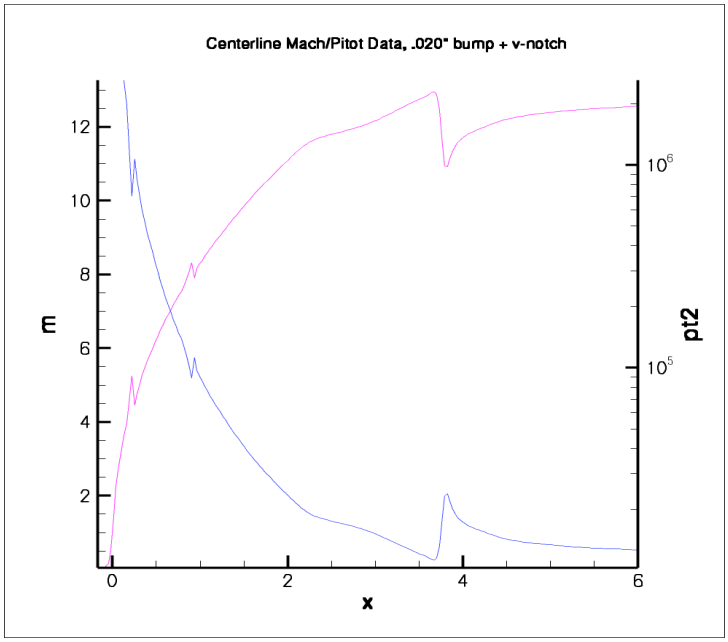

Figure 12. Centerline Mach and pitot pressure data for simulation with both joints.

4.4.2 Comparison of Flow Data

Figures 13 and 14 show the Pitot pressure distributions at multiple locations in the test cell for the simulation with both joints as compared to experimental data as well as simulation data using nominal nozzle geometry and a characteristics-based grid.

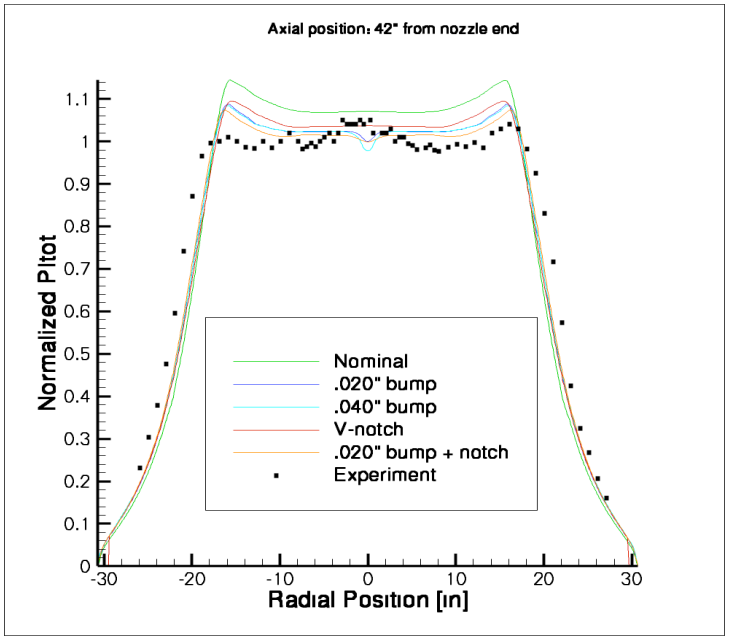

Figure 12. Pitot pressure data 42” into the test cell.

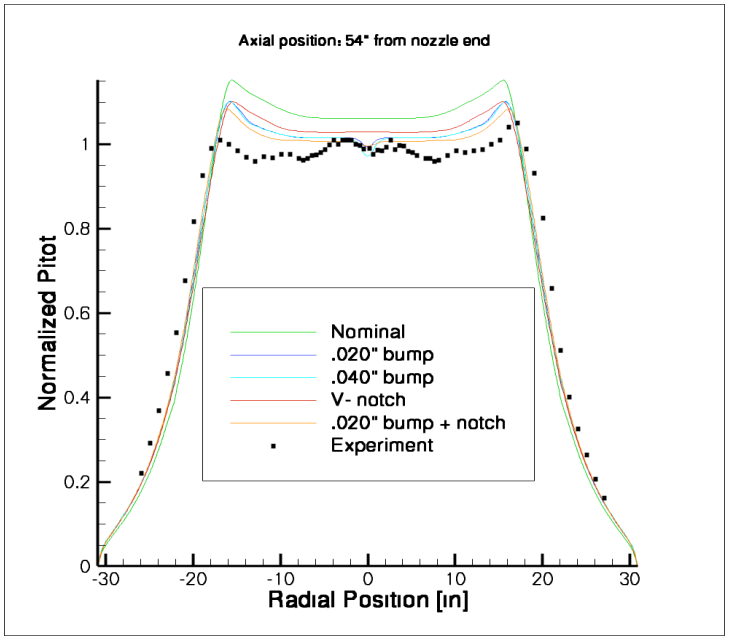

Figure 13. Pitot pressure data 54” into the test cell.

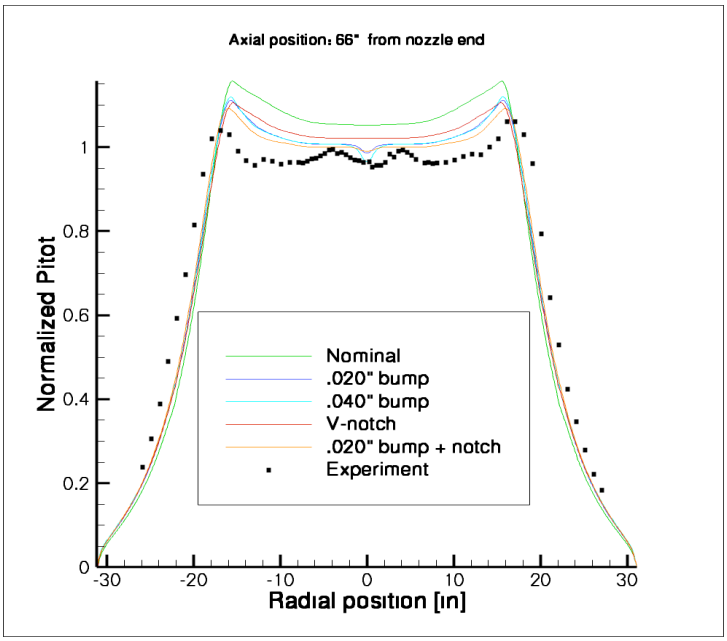

Figure 14. Pitot pressure data 66" into the test cell.

These plots demonstrate some key points. First, the waves generated by the joints cause significant losses in the Pitot pressure as compared to ideal geometry. Interestingly, increasing the size of the step height does not have a very significant effect on the overall Pitot pressure loss. It is possible that there is a critical height for which a wave will form, and increasing the height further will change the location the wave settles at rather than increasing its strength.

Also note that while there is a combinatorial effect of the waves generated by the two joints, it is not additive. The loss in Pitot pressure for the combined case is less than the sum of the losses for the individual cases. Additionally, there are still unexplained discrepancies between the computed Pitot pressure profile and the experimental results. There may be additional nozzle imperfections causing losses or variations in the Pitot pressure that have not been taken into account during this study.

5 Summary and Outlook

A grid generation scheme has been developed in which the grid elements can be aligned and refined near joint imperfections and the waves generated by them in the Tunnel 9 Mach 14 nozzle. This technique offers advantages that have allowed us to capture the effect of waves in the flow that have previously eluded us. This has led to a plausible explanation for some of the loss of Pitot pressure in the flow.

However, there is still significant disagreement between simulation and experimental for this data for this problem. In order to fully understand the test section core flow, additional research into the tunnel flow needs to be done. It may be necessary to include more as-built tunnel details into the simulations to accurately capture the real flow. Some of these details may require a multidimensional (rather than axisymmetric) approach. Overall, current results are not definitive, but they are promising regarding the possibility of understanding the Mach 14 nozzle flow in the future.

References

[1] Korte, J.J. E. Hedlund, S. Anandakrishnan, "A Comparison of Experimental Data with CFD for the NSWC Hypervelocity Wind Tunnel No. 9 Mach 14 Nozzle," AIAA-1992-4010, July 1992.

[2] Rao, M., A Collier, and T. Hand, "Design and Manufacture of the AEDC Tunnel 9 Aerodynamic Mach 8 Nozzle," AIAA Paper 2006-2812, June, 2006.

[3] Smith, M., and J. Coblish, "Measurements to Assess the Degree of Thermal Nonequilibrium at AEDC Hypervelocity Tunnel No. 9," AIAA Paper 2004-2399, June 2004.

[4] Smith, M. "Raman Density and Gas-Sampling Measurements During Tunnel 9 Mach 8 Calibration," AIAA-2006-2814.

[5] Nompelis, I., T.W. Drayna, and G.V. Candler, "Development of a Hybrid Unstructured Implicit Solver for the Simulation of Reacting Flows Over Complex Geometries," AIAA-2004-2227, June 2004.

[6] Nompelis, I., T.W. Drayna, and G.V. Candler, "A Parallel Unstructured Implicit Solver for Hypersonic Reacting Flow Simulation," AIAA-2005-4867, June 2005.

[7] Wright, M.J., D. Bose, and G.V. Candler, "A Data-Parallel Line Relaxation Method for the Navier-Stokes Equations," AIAA Journal, Vol. 36, No. 9, 1603-1609, Sept. 1998.

[8] Meador, W.E., L.W. Townsend, and G.A. Miner. "Effects of H_2O Vapor on Vibrational

Relaxation in Expanding and Contracting Flows," AIAA-1996-0105, Jan. 1996.

[9] Candler, G.V., "Hypersonic Nozzle Analysis Using an Excluded Volume Equation of State," AIAA-2005-5202, June 2005.

[10] Vincenti, W.G., and C.H. Kruger, *Introduction to Physical Gas Dynamics*, Krieger Publishing Company, 1965.

[11] Bass, H.E. "Absorption of Sound by Air: High Temperature Predictions," *J. Acoust. Soc. Am*. Vol. 69, 1981, pp. 127-128.

[12] Nagel, J., and D. Rogovin. "V-V Exchange Involving H_20 Molecules: A Calculation of the N_2*-H_2O Deactivation Rate Constant," *J. Chem. Phys*., Vol. 72, No. 12, 1980, pp. 6593-6601.